Solution structures of the C-terminal headpiece subdomains of human villin and advillin, evaluation of headpiece F-actin-binding requirements

WIM VERMEULEN,[1] PETER VANHAESEBROUCK,[1] MARLEEN VAN TROYS,[2] MIEKE VERSCHUEREN,[1] FRANKY FANT,[1] MARC GOETHALS,[2] CHRISTOPHE AMPE,[2] JOSÉ C. MARTINS,[1] AND FRANS A.M. BORREMANS[1]

[1]NMR and Structure Analysis Unit, Department of Organic Chemistry, Faculty of Sciences, Ghent University, 9000 Ghent, Belgium

[2]Department of Biochemistry, Faculty of Medicine and Health Sciences, Ghent University and Department of Medical Protein Science, Flanders Interuniversity Institute for Biotechnology (VIB09), 9000 Ghent, Belgium

(RECEIVED November 19, 2003; FINAL REVISION February 12, 2004; ACCEPTED February 14, 2004)

Abstract

Headpiece (HP) is a 76-residue F-actin-binding module at the C terminus of many cytoskeletal proteins. Its 35-residue C-terminal subdomain is one of the smallest known motifs capable of autonomously adopting a stable, folded structure in the absence of any disulfide bridges, metal ligands, or unnatural amino acids. We report the three-dimensional solution structures of the C-terminal headpiece subdomains of human villin (HVcHP) and human advillin (HAcHP), determined by two-dimensional ^{1}H-NMR. They represent the second and third structures of such C-terminal headpiece subdomains to be elucidated so far. A comparison with the structure of the chicken villin C-terminal subdomain reveals a high structural conservation. Both C-terminal subdomains bind specifically to F-actin. Mutagenesis is used to demonstrate the involvement of Trp 64 in the F-actin-binding surface. The latter residue is part of a conserved structural feature, in which the surface-exposed indole ring is stacked on the proline and lysine side chain embedded in a PXWK sequence motif. On the basis of the structural and mutational data concerning Trp 64 reported here, the results of a cysteine-scanning mutagenesis study of full headpiece, and a phage display mutational study of the 69–74 fragment, we propose a modification of the model, elaborated by Vardar and coworkers, for the binding of headpiece to F-actin.

Keywords: headpiece subdomain; villin; advillin; NMR solution structure; actin-binding protein

Supplemental material: see www.proteinscience.org

Headpiece (HP) is an ~76-residue F-actin-binding domain present at the C terminus of many otherwise unrelated proteins (Vardar et al. 1999). It was first discovered in the epithelial brush border protein villin, a member of the gelsolin family, which consists of six gelsolin repeats, followed by the C-terminal headpiece domain (Glenney et al. 1981; Arpin et al. 1988; Bazari et al. 1988). In vitro, villin has been demonstrated to bundle and sever F-actin (Bretscher

Reprint requests to: José C. Martins, NMR and Structure Analysis Unit, Department of Organic Chemistry, Faculty of Sciences, Ghent University, Krijgslaan 281 S4, 9000 Ghent, Belgium; e-mail: jose.martins@UGent.be; fax: 32-9-264-49-72; or Christophe Ampe, Department of Biochemistry, Faculty of Medicine and Health Sciences, Flanders Interuniversity Institute for Biotechnology (VIB09), Albert Baertsoenkaai 3, 900 Ghent, Belgium; e-mail: christophe.ampe@UGent.be; fax: 32-9-264-94-88.

Abbreviations: CD, circular dichroism; cHP, C-terminal headpiece subdomain; CVcHP, chicken villin C-terminal headpiece subdomain; CVHP67, chicken villin headpiece without N-terminal linker; DQF-COSY, double quantum filtered correlation spectroscopy; DSS-d6, 2,2-dimethyl-2-sila 3,3,4,4,5,5-hexadeutero-pentane sulphonic acid; DTT, dithiothreitol; E.COSY, exclusive correlation spectroscopy; HP, headpiece; HAcHP, human advillin C-terminal headpiece subdomain; HVcHP, human villin C-terminal headpiece subdomain; NOE, nuclear Overhauser effect; NOESY, nuclear Overhauser effect spectroscopy; rEM, restrained energy minimization; rMD, restrained molecular dynamics; r.m.s.d., root-mean-square deviation; TOCSY, total correlation spectroscopy; TPPI, time proportional phase incrementation; TrisHCL, [tris-(hydroxymethyl)aminomethane]hydrochloride.

Article and publication are at http://www.proteinscience.org/cgi/doi/10.1110/ps.03518104.

and Weber 1980; Craig and Powell 1980; Mooseker et al. 1980; Glenney and Weber 1981). The bundling activity is critically dependent on the F-actin-binding capacity present in the headpiece domain (Zhai et al. 2001). Advillin (or pervin) is the closest relative of villin and has a similar domain structure. It plays an important role in regulating process outgrowth in peripheral neurons, and this requires the presence of the putative actin-binding headpiece domain (Ravenall et al. 2002).

The structure of chicken villin HP67 (containing the last 67 residues of headpiece; Vardar et al. 1999) revealed that the headpiece domain is composed of an N-terminal and a C-terminal subdomain (cHP). Prior to this, it was shown (McKnight et al. 1996, 1997) that the C-terminal subdomain of chicken villin autonomously folds into a stable structure in solution, bearing a unique fold topology that consists of three helices packed around a hydrophobic core. The structure of this isolated cHP is highly similar to its structure in the full headpiece, with differences mainly confined to the N- and C-terminal residues and the residues implicated in the interaction with the N-terminal subdomain (Vardar et al. 1999). Thus, the forces that induce the structuring of the chicken villin cHP appear largely present within the subdomain itself, giving the cHP the status of a mini-protein.

By mapping the results of a cysteine-scanning mutagenesis study (Doering and Matsudaira 1996) on the chicken villin HP67 structure, a model for F-actin binding was proposed. Most of the residues involved in this interaction are located in the third helix of the C-terminal subdomain. On this basis, and given the structure of the chicken villin headpiece, it was proposed that F-actin-binding headpieces contain three essential structural features formed by generally conserved residues (Vardar et al. 1999) as follows: a surface-exposed hydrophobic patch dominated by Trp 64, a band of alternating charges, termed crown, surrounding this patch, and a positive patch below the charged crown. More recently, however, Rossenu et al. (2003) showed that part of the charged crown residues are dispensable for actin binding. Surprisingly, the functional importance of Trp 64 for F-actin binding was never experimentally investigated.

Until now, the structure of only one C-terminal headpiece subdomain is known (chicken villin) and structural conservation of the subdomain in related headpieces is assumed on the basis of sequence conservation. This requires that the cHP-fold should be tolerant to changes in sequence composition.

We determined the structures of a second and third cHP, namely of human villin and advillin, as representatives with 74% and 60% sequence identity to the chicken villin cHP. We show that these two C-terminal headpieces indeed form stable subdomains having very similar packing, despite conservative mutations in the hydrophobic core. In addition, we show that the C-terminal headpiece subdomain of advillin binds filamentous actin and that Trp 64 contributes to actin interaction. In view of the results presented here, and guided by data from a recent mutational analysis of part of the last helix in headpiece by a phage display method (Rossenu et al. 2003), the Vardar model for the F-actin-binding site (Vardar et al. 1999) is evaluated and modifications are proposed.

Results and Discussion

The C-terminal subdomain of advillin binds to F-actin, Trp 64 is involved in actin binding

We synthesized two peptides representing the C-terminal subdomains of human villin (HVcHP) and advillin (HAcHP). These start, respectively, at residue 42 and 41 compared with the full-length HP. To assess the F-actin-binding activity of these peptides, we used chemical cross-linking, followed by sedimentation. Assuming similar cross-linking efficiencies, this semiquantitative approach allows the evaluation of relative binding affinities of the headpieces from the amount of headpiece coupled to actin molecules in the filament and, hence, retrieved in the pellet fraction after sedimentation. The cross-linking step is required, as binding of the C-terminal headpiece subdomains is relatively weak (Vardar et al. 2002). Figure 1 shows an SDS-PAGE analysis of the pellet fraction of samples in which increasing concentrations of HVcHP (top) or HAcHP (middle) were added to F-actin. The cross-linked complex, migrating with slightly lower mobility, appears in both cases already at 12 μM (i.e., when added in a 1 : 1 molar ratio to actin protomers) and is very prominent at 60 μM. This indicates that the C-terminal subdomains of human villin and advillin interact with similar affinities with actin filaments.

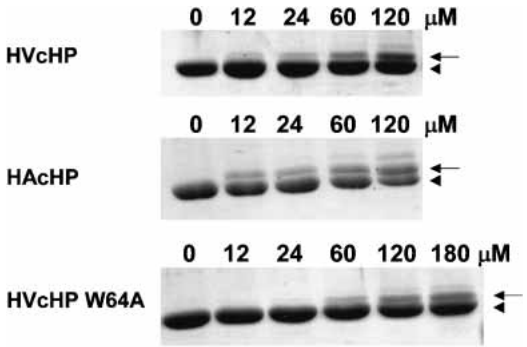

Figure 1. SDS-PAGE of sedimented F-actin with EDC-cross-linked headpiece subdomains (for experimental details, see Materials and Methods). The concentrations of HVcHP, HAcHP, and HVcHP W64A used are indicated *above* each lane. The bands corresponding to actin only (arrowhead) and actin bound to peptide (arrow) are indicated. Binding efficiency is reflected by the concentration of peptide necessary for the appearance of the slower migrating F-actin-peptide band.

Given our identification of a conserved local structural motif around Trp 64 (see below) and the important role hypothesized for this residue in actin binding in a currently proposed headpiece F-actin-binding model (Vardar et al. 2002), we also tested a variant of HVcHP in which Trp 64 is substituted by Ala (Fig. 1, bottom). F-actin binding by this mutant is strongly reduced compared with wild-type HVcHP, as cross-linking is only apparent upon addition of 60 μM of the peptide. Given that this mutant adopts an otherwise wild-type-like folded structure (see below), this presents the first actual evidence for a pivotal role for Trp 64 in F-actin interaction.

Human villin, advillin, and villin mutant Trp64Ala C-terminal subdomains have similar secondary structures and stable folds

NMR structural analysis was done at pH 4.2, as the subdomains were insoluble at physiological conditions (pH 7.0, 10 mM phosphate buffer) at the concentrations used (2 mM). However, CD-spectra at lower concentrations (40 μM) taken at pH 4.3, 6.0, and 7.5 were similar (data not shown), suggesting that the structure of both cHPs is not grossly influenced by pH.

Initial inspection of the NMR spectra of the cHPs showed a good chemical-shift dispersion in the amide region, and a large number of cross-peaks in the NOESY spectra, demonstrating that each peptide adopts a folded structure under the conditions used.

Nearly complete sequence-specific resonance assignments were obtained for all three peptides (HVcHP, HAcHP, and HVcHP Trp 64Ala) at a single temperature (294 K). All residues were sequentially assigned via a continuous stretch of d_{NN}, $d_{\alpha N}$, and/or $d_{\beta N}$ NOE contacts. All peptide bonds involving an Xxx-Pro segment were in the *trans* conformation, as evidenced by the presence of strong sequential $d_{\alpha\delta}$ NOE contacts. Most of the exchangeable protons in Lys/Arg side chains could not be identified, due to fast exchange with the solvent.

As is shown by the NMR data (Fig. 2), the three subdomains studied adopt a similar fold, composed of three α-helices. Analysis of the NOESY spectra resulted in the collection of 629 distance restraints for the human villin cHP and 784 for the human advillin cHP, of which 23%, respectively, 21% were long range (Table 1). The average number of 18 and 22 restraints per residue, respectively, indicates that these peptides adopt a compact structure, amenable to high-resolution structure determination by ^{1}H-NMR.

Three-dimensional structure calculations and quality of the structures

The solution structures of human villin cHP and human advillin cHP are represented by an ensemble of 25 refined conformers each, and are shown in Figure 3. Structures were calculated with DYANA (Güntert et al. 1997), using the REDAC strategy, and refined using a simulated annealing protocol in the AMBER force field (Weiner et al. 1984). The average target function values of 0.58 Å^2 and 0.48 Å^2 for the human villin cHP and human advillin cHP ensemble, respectively, indicate that they are in excellent agreement with the experimental data. The ensemble calculation statistics before and after refinement are presented in Table 1. As can be expected, the main improvement upon refinement concerns the van der Waals interactions. The refined structures have very few NOE violations larger than 0.2 Å and few dihedral angle violations larger than 5°. Nearly all residues have backbone φ and ψ angles in the most favored regions of the Ramachandran plot according to PROCHECK-NMR (Laskowski et al. 1996).

Disregarding the acetylated N-terminal residues and the C-terminal phenylalanine in both structure ensembles, the collection of conformers converge to the same overall fold (Fig. 3). The r.m.s.d. values for the backbone atoms are 0.72 Å (± 0.29) and 0.52 Å (± 0.25) for the HVcHP and HAcHP peptide, respectively. For all heavy atoms, the r.m.s.d. values are 1.27 Å (± 0.25) and 1.04 Å (± 0.22). The structures of both subdomains are well defined at the secondary structure level including both loops (52–54 and 61–62). The N and C termini are ill defined, owing to the lack of long-range NOE contacts involving these parts of the sequence. The circular variance of the χ^1 torsion angles of the residues in the hydrophobic core (see below) in the human villin cHP ensemble is not larger than 0.025 (except for M53, which adopts two conformers in the ensemble), and not larger than 0.006 in the human advillin cHP. The circular variance of the χ^2 torsion angles of these residues is not larger than 0.160 and 0.216 in the respective ensembles. These rather low values, in particular for χ^1 variance, show that the side chains in the hydrophobic core are determined with good precision, allowing a comparison of their orientation between cHP structures. Similarly, the overall low circular variance of the χ^1 and χ^2 angles of Thr 54, Trp 64, Lys 65, and Gln 66 allowed the assessment of their functional or structural role in the headpiece subdomain (see below).

Description of the three-dimensional structures of the villin and advillin C-terminal headpiece subdomains and comparison with chicken villin cHP and chicken villin HP67

The C-terminal headpiece subdomains of human villin and advillin adopt a compact, well-defined globular fold with three α-helices (Fig. 3). The first α-helix starts at residue 44 (Ile/Glu) in both structures and ends with residue 51 (Phe). A short loop of three residues (Gly 52–Thr 54) coiling back over this helix connects it to the second and shortest helix of cHP and places both helices perpendicular to each other.

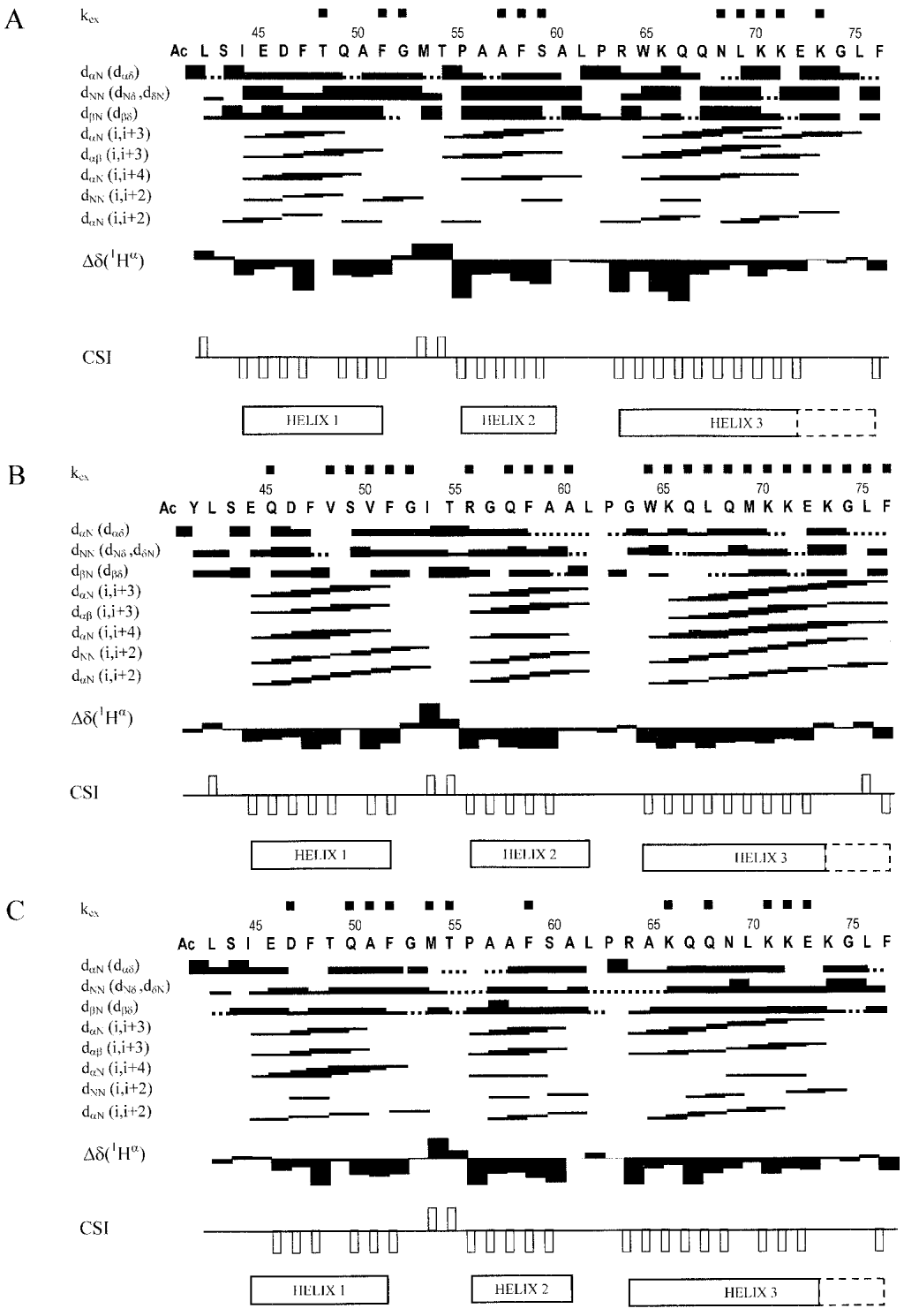

Figure 2. Secondary structures of (*A*) HVcHP, (*B*) HAcHP, and (*C*) HVcHP W64A derived from NMR data, represented according to IUPAC recommendations (Markley et al. 1998). *Above* the amino acid sequence (Ac indicates the acetyl group), black squares identify residues with low-backbone amide hydrogen exchange rates, k_{ex}. Weak to strong sequential NOE intensities are represented by thin to thick bars *below* the sequence. Dots indicate NOE contacts with uncertain cross-peak intensity due to cross-peak overlap. Unambiguously assigned medium range NOE contacts are represented by lines. $^1H^\alpha$ shifts relative to random coil values and the Chemical Shift Index (CSI; Wishart et al. 1992) are indicated. Sequence locations of the helices are shown at the *bottom*; broken lines indicate that the location of the C terminus of helix 3 from these data is uncertain.

Table 1. *Structure calculation statistics*

	HVcHP		HAcHP	
	DYANA	refinement	DYANA	refinement
Restraints (number)				
Distance total (upper)		629		784
intraresidue		146		191
sequential		134		188
medium range		204		239
long range		145		166
H-bond (upper/lower)[a]	22/22	0/0	28/28	0/0
Dihedral angles (number)[b]				
ϕ	52	32	51	34
ψ	47	32	41	35
χ^1	41	23	40	27
Stereospecific assignments (number)				
β methylene group		12		16
other methylene groups		4		3
γ methyl groups for valine		0		2
δ methyl groups for leucine		2		1
amide side chains Gln/Asn		4		3
Target function ($Å^2$, DYANA)[c]	0.58 ± 0.05		0.48 ± 0.04	
Energy (kcal · $mole^{-1}$)[d]				
total	[e]	−150.4 ± 5.4	[e]	−142.8 ± 5.1
bond lengths	[e]	5.1 ± 0.3	[e]	6.3 ± 0.2
angles	[e]	36.5 ± 1.2	[e]	37.4 ± 1.3
impropers	[e]	51.9 ± 2.2	[e]	44.7 ± 8.5
van der Waals	446.2 ± 506.1	−127.9 ± 3.1	2656.2 ± 4630.0	−126.1 ± 3.6
electrostatics	−79.1 ± 7.7	−100.8 ± 3.5	−85.7 ± 6.8	−94.2 ± 4.7
hydrogen bonds		−16.4 ± 0.8		−14.1 ± 0.7
No. of dist. restr. viol. >0.2 (Å)	0.6 ± 0.5	0.2 ± 0.4	0.2 ± 0.4	>0.1 ± 0.2
No. of angle restr. viol. >5.0 (°)	0.0 ± 0.0	3.0 ± 0.9	0.0 ± 0.0	7.1 ± 1.6
Ramachandran plot				
(%) of residues				
in most favored regions		96.8		91.6
in additionally allowed regions		3.2		8.0
in generously allowed regions		0.0		0.4
in disallowed regions		0.0		0.0

Results of 25 conformers with lowest Target Function value (DYANA, Güntert et al. 1997)
[a] Hydrogen bond restraints were omitted during refinement.
[b] Multiple restraints for a single torsion angle were reduced to a single restraint during refinement.
[c] 1 Å = 0.1 nm.
[d] 1 cal = 4.184 J.
[e] Not included, as the original conformers have the ECEPP/2 standard geometry.

This second helix, which starts at residue 55 (Pro/Arg) and ends with alanine 60, contains two helical turns, of which the second adopts a 3_{10} type conformation. A second short non-β-turn loop (residues Leu 61 and Pro 62), connects the second helix to the last. This third and longest α-helix comprises residues 63–72 in HVcHP and 63–74 in the HAcHP.

With 74% and 60% sequence identity, the global fold of HVcHP and HAcHP is very similar to the fold of the chicken villin cHP (CVcHP; PDB accession code 1VII; McKnight et al. 1997) and the C-terminal subdomain in the chicken villin full domain (CVHP67; PDB accession code 1QQV; Vardar et al. 1999), as shown in Figure 5A, below. For structural comparison, all backbone atoms (with the exception of the first and last residue) of the average structures from each ensemble were aligned. The r.m.s.d. values show that all structures are similar (1.80 Å for HVcHP-HAcHP, 2.42 Å for HVcHP-CVcHP, 2.68 Å for HVcHP-CVHP67, 2.33 Å for HAcHP-CVcHP, and 2.32 Å for HAcHP-CVHP67). Limiting the extent of alignment to fragment 44–70 yields a much better fit (1.19 Å for HVcHP-HAcHP, 2.02 Å for HVcHP-CVcHP, 2.17 Å for HVcHP-CVHP67, 1.64 Å for HAcHP-CVcHP, and 1.64 Å for HAcHP-CVHP67). Thus, in addition to some small structural differences, the structure of the central core fragment is very similar at the backbone level in all isolated and incorporated (CVHP67) C-terminal subdomains.

Larger structural differences exist between the cHPs at the N and C termini. These are likely to be due to a lower

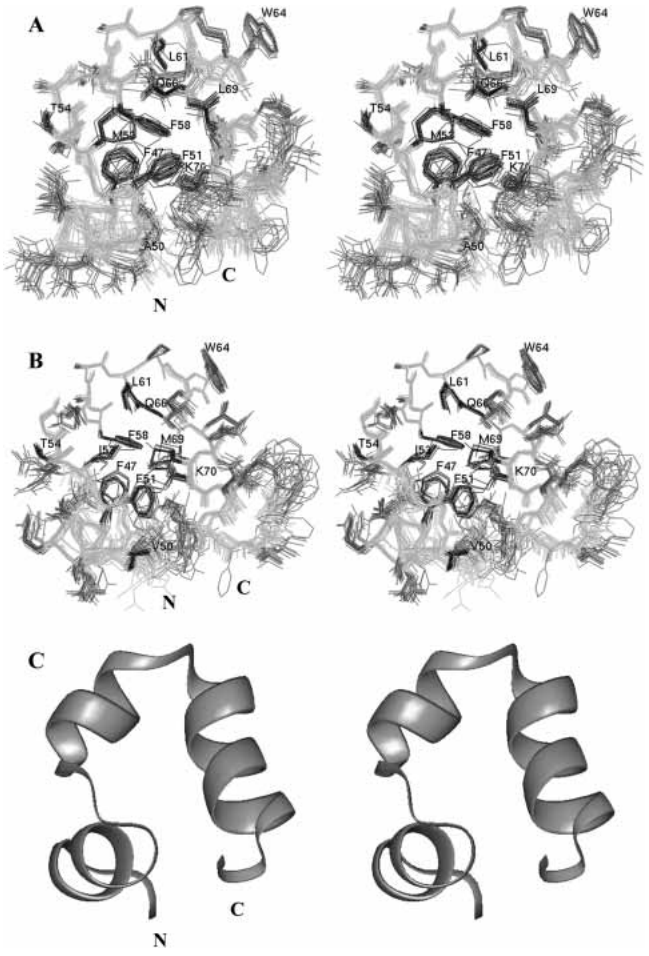

Figure 3. Stereoview of ensembles representing the three-dimensional structures of HVcHP and HAcHP. (*A*) Backbone superposition of 25 refined HVcHP structures. The backbone is shown in light gray. W64 and the conserved side chains important for fold stability are labeled and colored black; other side chains are shown in gray. (*B*) Backbone superposition of 25 refined HAcHP structures represented as in *A*. (*C*) Ribbon representation of the secondary structure elements of the HVcHP first structure in the ensemble.

accuracy of the structure determinations in these fragments, which could result from inherent flexibility of the termini in the isolated cHP.

Residues that contribute to fold stability

The structure of CVcHP remains largely the same when the N-terminal subdomain is present (Vardar et al. 1999), and the two structures determined here show that the fold is well conserved and unaffected by the sequence variability. Thus, the C-terminal headpiece subdomain can truly be viewed as a mini-protein, its sequence containing the necessary elements to fold autonomously into a stable structure.

A total of 10 residues contribute to the formation of the hydrophobic core as follows: Leu 42, Phe 47, Val/Ala/Val 50 (CVcHP, HVcHP, and HAcHP), Phe 51, Met/Met/Ile 53, Phe 58, Leu 61, Lys 65, Leu/Leu/Met 69, and Lys 70. Mutations occurring at these positions are conservative and yield similar side-chain orientations, thus minimizing perturbations to the hydrophobic core. The fact that natural mutations infrequently occur at positions 47, 51, 58, and 61 (Fig. 4), suggests that these residues are important determinants of the cHP-fold. The higher mutational tolerance at positions 50, 53, and 69 indicates that these residues provide only additional contributions to fold stability. Although involved in the hydrophobic core, strict conservation of Leu 42 and Lys 70 appears not to be essential for cHP fold stability. Their mutational invariance rather serves the stability of full headpiece as was suggested before (Vardar et al. 1999). Lys 65 is strictly conserved for F-actin binding (vide infra).

Additionally, conserved hydrophilic residues may also increase fold stability. First, in both structure ensembles $O^{\gamma 1}$ of Thr 54 is involved in hydrogen bonding to the backbone NH of Ala/Gln 57 (Fig. S, supplementary material). This is confirmed by the high protection of the backbone NH of residue 57 from hydrogen/deuterium exchange. Therefore, it is most likely that Thr/Ser 54 serves as an N-capping residue for the second helix. We note that at position 54, threonine or serine is found in the majority of the known headpiece sequences (Fig. 4). Second, residue Gln 66 is wedged between helix 2 and helix 3, and one side-chain amide proton ($H^{\epsilon 22}$) forms a hydrogen bond with the backbone CO of Leu 61 (Fig. S, supplementary material). A long side chain with a H-donor at the end (Gln/Arg/Lys; see Fig. 4) is needed to accomplish such a hydrogen bond. This residue presumably contributes to fold stability by interacting favorably with the $\beta_p\beta_p$ loop and the dipole of helix 2. Because the second helix is the shortest and, therefore, on its own, the least stable of the three helices, it is likely that its formation, and concomitantly, the proper adoption of the subdomain structure, is enhanced by the presence of these N-capping (Thr 54) and helix dipole stabilizing (Gln 66) residues.

Structure vs. biological activity

Above, we demonstrated that Trp 64 contributes to actin binding. The present NMR data provide strong support for the involvement of Trp 64 in a direct contact with F-actin. First, the secondary structure of the Trp64Ala mutant corresponds to that of HVcHP (Fig. 2), and the same long-range NOE contacts are found between residues in the hydrophobic core (data not shown), indicating that the structure of the mutant is highly similar to wild type. Because chemical shifts provide a sensitive probe for subtle structural changes, we also compared the proton chemical shifts of HVcHP with those of the Trp64Ala mutant. Differences larger than 0.1 ppm were almost exclusively found for pro-

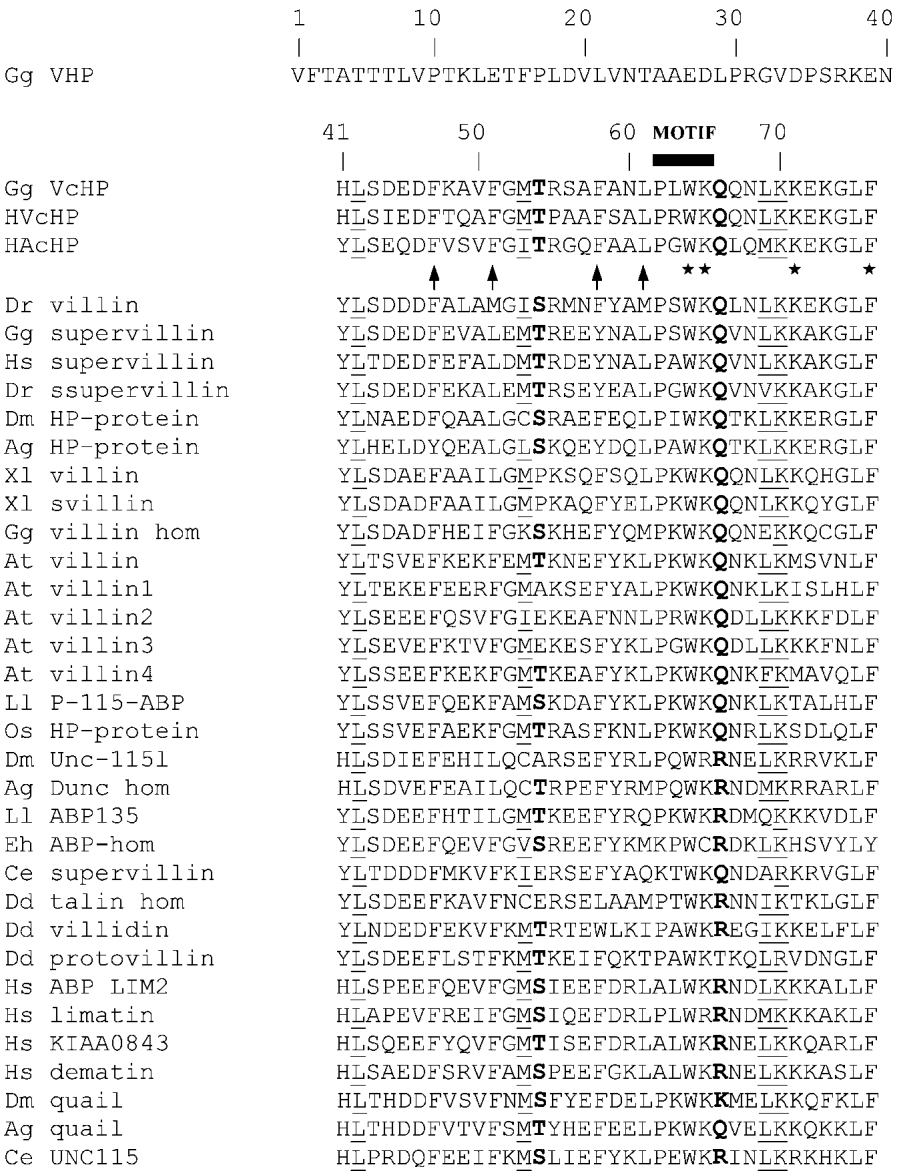

Figure 4. Sequence alignment of HVcHP, HAcHP, and 31 additional C-terminal headpiece subdomains with respect to chicken villin headpiece (numbering is according to McKnight et al. 1996). Residue positions that are strongly conserved for cHP fold stability (see text) are indicated by arrows below the HAcHP sequence. Residues conserved for fold stability via contributions of hydrophobic and hydrophilic side-chain moieties (see text) are shown underlined and in bold, respectively. Residues conserved for F-actin binding are indicated by stars below the HAcHP sequence. The PXWK motif (see text) is indicated by a black bar. The additional C-terminal headpiece subdomain sequences were retrieved from the nonredundant protein database at http://www.ncbi.nlm.nih.gov/entrez or translated from cDNA or EST-sequence entries. Database annotations were used to name the proteins; in the case of *Anopheles gambiae*, this is based on similarities with *Drosophila melanogaster* proteins. If the function of the protein is unknown, it is referred to as headpiece-containing protein (name, accession no.): chicken villin headpiece (Gg VHP, A31822), human villin (HVcHP, CAA00664), human advillin (HAcHP, NP 006567), *Danio rerio* villin (Dr villin, AAH47186), chicken supervillin homolog (Gg supervillin, BU261201), human supervillin (Hs supervillin, AAC64695), *D. rerio* similar to supervillin (Dr ssupervillin, AI958855), *D. melanogaster* headpiece-containing protein (Dm HP-protein, NP 647726), *A. gambiae* headpiece-containing protein (Ag HP-protein, XP 308589), *Xenopus laevis* similar to villin (Xl villin, AAH44966), *X. laevis* similar to villin (Xl svillin, AAH45214), chicken villin homolog (Gg villin hom, BX277781), *Arabidopsis thaliana* villin (At villin, NP 200542), *A. thaliana* villin 1 (At villin1, AAC31605), *A. thaliana* villin 2 (At villin2, AAC31606), *A. thaliana* villin 3 (At villin3, AAC31607), *A. thaliana* villin 4 (At villin4, O65570), *Lilium longiflorum* actin-binding protein P-115-ABP (Ll P-115-ABP, BAC77209), *Oryza sativa* headpiece-containing protein (Os HP-protein, CB097108), *D. melanogaster* Unc-115l (Dm Unc-115l, AAL30427), *A. gambiae* homolog of *D. melanogaster* Unc-115l (Ag Dunc hom, XP 315432), *L. longiflorum* actin-bundling protein ABP135 (Ll ABP135, AAD54660), *Entamoeba histolica* actin-binding protein homolog (Eh ABP-hom, AAD30430), *Caenorhabditis elegans* supervillin (Ce supervillin, NP 491442), *Dictyostelium discoideum* talin homolog (Dd talin hom, BAA75511), *D. discoideum* villidin (Dd villidin, CAD20809), *D. discoideum* protovillin (Dd protovilin, P36418), human actin-binding LIM2 protein (Hs ABP LIM2, NP 115808), human limatin (Hs limatin, NP 00671), human KIAA0843 (KIAA0843, NP 055760), human dematin (Hs dematin, AAC64695), *D. melanogaster* Quail (Dm Quail, Q23989), *A. gambiae* Quail hom (Ag Quail, XP 320012), *C. elegans* UNC115 (Ce UNC115, NP 509702).

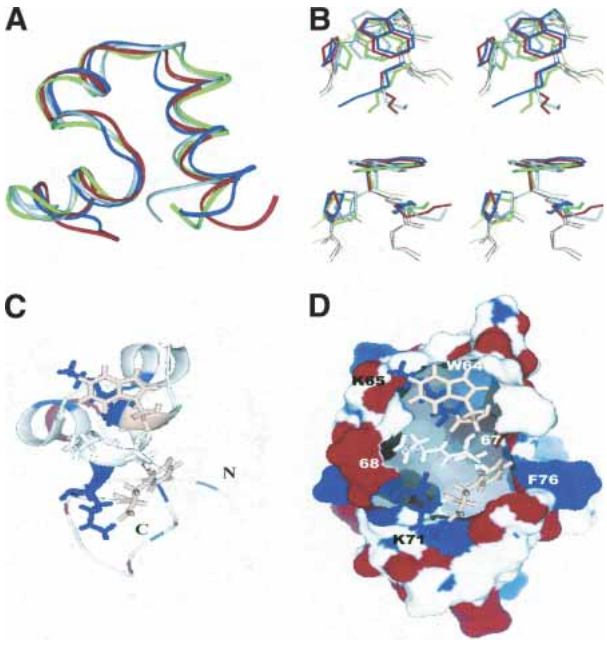

Figure 5. Superposition of headpiece C-terminal subdomains and model of the F-actin-binding site. (*A*,*B*) Superposition of HVcHP, HAcHP, and CVcHP (PDB code 1VII) on CVHP67 (PDB code 1QQV) shown in blue, red, gray, and green, respectively, highlighting structural similarity. The first structure of each conformer ensemble is used. (*A*) Ribbon drawing representing the backbone of the four C-terminal headpiece subdomains. The location of the PXWK motif (see text) is indicated by an arrow. The backbone atoms of residues 44–70 are superimposed. (*B*) Superposition of fragment 61–66 of the four structures, displaying the side chains of Pro 62, Trp 64, and Lys 65 as sticks. Stereoviews are perpendicular (*top*) and parallel (*bottom*) to the indole ring. (*C*,*D*) Model of the F-actin-binding site on headpiece displayed on the HP67 structure (PDB code 1QQV). Negatively charged residues are indicated in red; positively charged residues, in blue. Hydrophobic residues critical for F-actin binding are shown in pink. Residues involved in F-actin binding as well as residues 67 and 68 (see text) are labeled and displayed as sticks. (*C*) Ribbon representation with labeled N and C termini. (*D*) Surface potential representation.

tons close to the indole ring (residues 61–67), indicating that only local structural perturbations are caused. The reduced binding we observed is thus not due to gross structural changes and is consistent with the idea that this residue is at the F-actin-binding patch of headpiece. Second, comparison of the three cHP structures and the CVHP67 structure reveals a pronounced and conserved local structural feature consisting of the highly similar side-chain orientation and packing of Pro 62, Trp 64, and Lys 65, further referred to as the PXWK motif (Fig. 5B). One face of the indole ring is stacked against the aliphatic side chains of Pro and Lys, thus exposing the other face toward the solvent. To validate the accuracy of the structure determination in the PXWK motif, we calculated the chemical shifts from the ensemble coordinates, using the program SHIFTS 4.1 (http://www.scripps.edu/case/; Osapay and Case 1991; Case et al. 1995) and compared them with the observed chemical shifts. The structures of the cHPs reproduce a large part of the >0.3 ppm chemical-shift deviations (CSDs) from random coil values. For example, the observed CSD values of the Lys 65 NH, β_2, γ_2, and γ_3 protons of −2.24, −1.83, −0.66, and −0.49 ppm for the advillin peptide compares well with the calculated values (−2.22 ± 0.07, −1.90 ± 0.10, −0.65 ± 0.06, and −0.45 ± 0.04), respectively. With the exception of the β_2 proton, similar results are found for the human villin cHP peptide. Other large CSDs are not as well reproduced, but follow the same trend. Thus, keeping in mind the anisotropic nature of the ring current-induced shift, and the possibility of residual flexibility around the various torsion angles of the residues involved, the PXWK motif is an accurately determined feature of HP structures. Its evolutionary conservation is consistent with the important role of Trp 64 in F-actin binding.

Other residues in the PXWK motif were suggested to be involved in F-actin binding (Vardar et al. 2002). At position 65, a Lys residue is found in nearly all known headpiece sequences (Fig. 4). Furthermore, a Lys65Cys mutant displayed weakened interaction with F-actin (Doering and Matsudaira 1996). It remains to be evaluated whether this is caused by loss of a direct interaction or by a changed local stacking of Trp 64. It was argued (Vardar et al. 2002) that the presence of a relatively long aliphatic side chain at position 63 (X in PXWK motif) may be necessary for tight binding, as it is found in headpieces displaying high-affinity interaction with F-actin (human and chicken villin and dematin headpiece), whereas it is absent in low-affinity headpieces (supervillin, villidin, and protovillin headpiece). However, we find that F-actin binding by HAcHP, containing glycine at this position, is not markedly different from HVcHP. Therefore, the contribution of this residue to F-actin binding is questionable.

A model was suggested detailing the binding of headpiece on F-actin (Vardar et al. 1999). It combined structural results using the CVHP67 structure, affinity measurements of selected headpieces (Vardar et al. 2002), and results from a limited cysteine-scanning mutagenesis study (Doering and Matsudaira 1996). They proposed three critical features for high-affinity F-actin-binding headpieces; first, Leu 63 and Trp 64 contribute to the formation of a hydrophobic patch termed the "cap"; second, Arg 37, Lys 65, Lys 71, Glu 72, and the carboxylate group of Phe 76 form a band of alternating charges surrounding the cap, referred to as the "crown"; thirdly, a positive patch containing residues Lys 38 and Lys 73 is located below the crown. In this model, headpiece binds by docking the hydrophobic cap onto actin, a proposal that is supported by the present data on Trp 64, and is locked in place by electrostatic interactions with the crown. Recent mutational analysis of the 69–74 region by phage display (Rossenu et al. 2003) has, however, shown that some of the charges in this model are not essential for binding to F-actin. Removal of the negative charge at po-

sition 72 has no pronounced effect on affinity. Also, mutation of Lys 73 does not deteriorate the binding with F-actin, and charge reversal (Lys73Glu) even increases binding strength. Furthermore, according to this analysis, the role of the C-terminal carboxylate is questionable, as the headpiece still binds to F-actin when presented as a C-terminal fusion protein. Thus, these phage-display results only indicate the requirement of Lys 71 for high-affinity binding to F-actin, the charged residues following Lys 71 appearing to be less important.

The absence of the three last amino acid residues in human villin significantly reduced its in vivo activities in transfected cells (Friederich et al. 1992). Leu 75 and Phe 76 are strictly conserved throughout all headpiece sequences. Both the Leu75Cys and Phe76Cys mutants display a significantly reduced actin-binding activity compared with wild type (Doering and Matsudaira 1996). Leu 75 is a core residue in CVHP67, and the observed decreased binding of the cysteine mutant may thus have a structural reason rather than abolishing a direct contact. In contrast, the side chain of Phe 76 is solvent exposed in CVHP67. This strongly suggests that this residue contributes to actin binding, but via hydrophobic interaction of its side chain rather than via the electrostatic interaction of its C-terminal carboxylate group, as was suggested (Vardar et al. 1999).

Also, on the basis of cysteine scanning, residues from the N-terminal domain have been proposed to partake of actin binding (Doering and Matsudaira 1996). In the structure of chicken villin HP67, the aliphatic part of the side chain of Lys 38 is part of the hydrophobic core, bridging both subdomains and making contact with conserved hydrophobic residues at position 21, 29, and 33 in the N-terminal subdomain and with Leu 75 in the C-terminal subdomain. Because only lysine or leucine is found at this position in other headpiece sequences (Fig. 4), this suggests that the presence of an aliphatic side chain at this position is a conserved element needed for structural stability. In this view, Lys 38 serves a somewhat similar function as the intersubdomain salt bridge formed by Glu 39 and Lys 70. Thus, we suggest that the lower affinity of the Lys38Cys mutant is due to structural instability, rather than the absence of a positive charge interacting favorably with F-actin. Our interpretation is supported by the observation that the absence of this charge in dematin (Vardar et al. 2002) and limatin (Roof et al. 1997) does not deteriorate high-affinity binding.

A second residue in the N-terminal domain, Arg 37, is part of the charged crown in the model of Vardar et al. (1999). However, mutation to Cys results in only a minor reduction of binding affinity (Doering and Matsudaira 1996). Therefore, although this residue can still be part of the binding site, the positive charge at position 37 does not seem to be critical for F-actin binding.

In light of this, we propose to modify the model proposed by Vardar for F-actin binding, to the following essential features (Fig. 5C,D): a hydrophobic patch, formed by Trp 64, two positive charges below the cap, originating from Lys 65 and Lys 71, and a second hydrophobic patch originating from the side chain of Phe 76. Because these four residues form two distinct patches on headpiece, it is tempting to speculate that the residues in between these patches, namely at position 67 and 68, also participate in the interaction with F-actin.

In conclusion, we have analyzed the structure and F-actin-binding capacity of the C-terminal headpiece subdomains of human villin and human advillin. By determining the structures of cHP subdomains from a second and a third villin family member, we verified the assumption that the structure of the subdomain is a stable folded protein module. The fold is tolerant to changes in sequence composition at selected positions, even in the core of the protein. Comparing the structures of HVcHP and HAcHP with the structure of the chicken villin subdomain (McKnight et al. 1997), and using sequence conservation arguments, enabled us to identify the residues that contribute to fold stability. In essence, residues at position 42, 47, 50, 51, 53, 58, 61, 65, 69, and 70 make up the hydrophobic core of cHP and residues at position 54 and 66, respectively, stabilize the second helix and the loop connecting the second and the third helix. On the basis of the present structural and functional data, combined with the data from a recent mutational analysis of the 69–74 fragment (Rossenu et al. 2003) and the cysteine scanning mutagenesis study (Doering and Matsudaira 1996), we suggest a model for F-actin binding of headpiece different from the one previously proposed (Vardar et al. 1999, 2002). In our model, Trp 64, Lys 65, Lys 71, and Phe 76 participate in F-actin binding, with Trp 64 and Phe 76 binding to complementary hydrophobic patches on actin, and Lys 65 and Lys 71 interacting favorably with negative charges on actin. This model only contains residues from the C-terminal subdomain, and we suggest that the N-terminal subdomain does not directly interact with actin. Instead, it serves to present the Phe 76 residue of the C-terminal subdomain to actin in a favorable conformation by fixing the C terminus via interaction with Leu 75, explaining the differences in binding affinity between isolated C-terminal headpiece subdomain and full headpiece.

Materials and methods

Peptide synthesis and purification

Following the chicken villin cHP (HP35, according to the nomenclature by McKnight et al. 1996) as a lead, N-acetylated fragments consisting of residues 792–826 of human villin and residues 784–819 of human advillin—that is, the C-terminal 35 or 36 residues of the headpiece—were synthesized on a model 431A peptide synthesizer (Applied Biosystems Inc.) using standard Fmoc-chemistry, following the instructions of the manufacturer. The peptides were purified using reversed-phase HPLC, and their correct iden-

tity was confirmed by mass spectrometry. The peptides were lyophilized and stored at −18°C until used. For binding assays, the peptides were dissolved in H_2O, neutralized, and their concentration was determined (Vancompernolle et al. 1992).

F-actin sedimentation assays

Monomeric Ca-ATP-G-actin was prepared from rabbit skeletal muscle (Spudich and Watt 1971) and further purified via Sephacryl S-300 (Pharmacia) in G-buffer (5 mM TrisHCl at pH 7.7, 0.1 mM $CaCl_2$, 0.2 mM ATP, 0.2 mM DTT, 0.01% NaN_3). For use in cross-linking, actin was dialyzed to the same buffer, except that TrisHCl was exchanged for phosphate. The G-actin (final concentration of 12 μM) was allowed to polymerize for 30 min at room temperature by adding KCl and $MgCl_2$ to final concentrations of 100 and 1 mM, respectively. Incubation of F-actin with HVcHP, HAcHP, or HVcHP Trp64Ala during 30 min at room temperature and 2 h at 4°C was followed by addition of the zero-length cross-linkers 1-ethyl-3(3-dimethylaminopropyl)carbodiimide (EDC, Sigma) and Sulfo-N-hydroxysuccinimide (Sulfo-NHS, Pierce) as described (Van Troys et al. 1996). After a 45-min reaction, the samples were spun at 100.000*g* (Beckman airfuge) for 10 min at room temperature to sediment actin filaments and associated headpiece subdomains. Supernatants and pellets were analyzed on 12.5% SDS–mini-slab gels (BioRad), followed by Coomassie staining. The concentration of the headpiece peptides used in these assays is shown in Figure 1.

NMR sample preparation, experiments, and resonance assignments

NMR samples were prepared by dissolving ~5.5 mg of lyophilized peptides in 90/10 H_2O/D_2O to a final concentration of ~2 mM. The pH was adjusted to 4.20 ± 0.05 (no correction was applied for the isotope effect) with minute amounts of NaOH and HCl. NaN_3 was used as an antibacterial agent, and dioxane for internal referencing (Wishart et al. 1995). When using DSS-d6 as reference compound, significant line broadening of its methyl resonances was observed, indicating intermolecular interaction with the peptides under the conditions used. Therefore, dioxane was used instead, as suggested before in such cases (Shimizu et al. 1994). The line width and chemical shift of the dioxane reference remained unaffected by the presence of cHPs.

All spectra were recorded at 500.13 MHz on a Bruker Avance-500 spectrometer operating at 294 K and equipped with a 5-mm SEI Z-gradient probe. Two-dimensional DQF-COSY (Rance et al. 1984; Neuhaus et al. 1985), NOESY (Kumar et al. 1980), and clean-TOCSY (Griesinger et al. 1988) experiments were performed with either States-TPPI (Marion et al. 1991; NOESY, DQF-COSY) or TPPI (Marion and Wüthrich 1983; clean-TOCSY) for phase-sensitive detection in f_1. Mixing times of 40, 80, 100, 150, and 200 msec were used for the NOESY spectra. For the TOCSY experiment, a 7.14-kHz spin-lock field was applied for 70 to 85 msec. Water suppression was achieved with WATERGATE (Piotto et al. 1992). E.COSY (Griesinger et al. 1985; Kessler and Oschkinat 1985; Eberstadt et al. 1995) spectra were recorded on D_2O samples of fully deuterium-exchanged HVcHP and HAcHP with TPPI phase-sensitive detection in f_1. The resulting 1024×512 time domain data matrices had a spectral width of 6010 or 7003 Hz in both dimensions. Spectral processing was done with XWINNMR 2.6. An initial baseline correction was done by convolution of the FID to suppress the residual water signal (Marion et al. 1989), followed by multiplication with a shifted ($\pi/4$ in f_1 and $\pi/3$ in f_2) squared sinebell function and zero filling. After Fourier transformation, a 5th order polynomial baseline correction was performed in both dimensions.

Sequence-specific assignments were achieved using the TOCSY, DQF-COSY, and NOESY spectra, following the sequential assignment procedure as described by Wüthrich (1986). $^3J_{\alpha H\text{-}NH}$-coupling constants were determined from the splitting of the cross-peaks in the DQF-COSY spectra according to the method of Kim and Prestegard (1989), whereas $^3J_{\alpha H\text{-}\beta H}$-coupling constants from the relative translation of subcross peaks in the E.COSY spectra. H/D exchange data were recorded at 294 K on samples prepared by adding D_2O to the lyophilized, hydrogenated peptide. One-dimensional spectra were recorded (36 experiments) at increasing time intervals for a total duration of 13 h (complete exchange) starting at 4–6 min after addition of D_2O.

Cross-peak assignment and general bookkeeping was done with Pronto (vs. 19990506; Kjær et al. 1994).

Secondary structure determination, structure calculation, and comparison

Secondary structures were determined by use of indicative NMR parameters. Sequential NOE contacts were classified as strong, medium, or weak on the basis of the number of contours in the 150 msec NOESY spectra. Random coil chemical shifts were obtained from Wishart and Nip (1998; D.S. Wishart, pers. comm.).

For structure calculation, cross-peak volumes were integrated with Pronto (Kjær et al. 1994). For the calculation of both structures, two NOESY spectra were used with 40- and 150-msec mixing times. Intraresidue NOE contacts, all sequential backbone contacts, and all sequential contacts involving methyl groups were integrated in the 40-msec NOESY spectrum, whereas all other contacts such as medium and long-range contacts were integrated in the 150-msec NOESY spectrum. Cross-peak volume conversion and subsequent structure calculation was performed within DYANA (version 1.5; Güntert et al. 1997). Cross peak volumes obtained from the 150 msec NOESY were converted to distance restraints using the macro CALIBA, which performs a standard calibration (Güntert et al. 1997). The 40-msec NOE cross-peaks were divided into three classes with calibration constants determined by using fixed distances as follows: N^H-H^β of alanine in an α-helix (3.40 Å), H^α_i-H^N_{i+1} in an α-helix (3.5 Å) and γCH_2 (1.74 Å), respectively. Pseudoatom corrections were applied to distance restraints involving nonstereospecifically assigned methylene, methyl, and aromatic protons (Wüthrich et al. 1983). Finally, all distance restraints were converted to upper limits by multiplication with 1.1. ϕ, φ, and χ^1 angle restraints were generated using HABAS on local backbone NOE restraints supplemented with $^3J_{H\alpha H\beta}$ coupling constants (10 for the HVcHP peptide and four for the HAcHP peptide) with values that agree with rigid χ^1 conformations (Nagayama and Wüthrich 1981). Stereospecific assignments of methylene protons and prochiral methyl groups (valine, leucine) were obtained either from HABAS grid-search analysis, from a statistical analysis of calculated structures, and/or from the application of GLOMSA in the final stages of structure calculation. Statistical analysis (Widmer et al. 1989) was done by comparing the allowed conformations generated by HABAS with the redundant angle restraints generated by REDAC (standard three-cycle schedule with 500, 1000, and 2000 steps). GLOMSA was performed with a cutoff and threshold of 0.4 Å, and stereospecific assignments were accepted if they were consistent in at least 80% of the structures. During the assignment process, typically 50 or 100 structures were calculated using the standard implementation

of torsion-angle dynamics. The 25 structures with lowest target function value were displayed for further assignment using the program InsightII (version 98.0, Accelrys, Inc.). At this stage, the structure calculations did not include the N-terminal acetyl group. Hydrogen-bond restraints (standard upper- and lower-distance restraints) were added in the later stages of structure calculation, and were based upon qualitative treatment of the hydrogen exchange data and inspection of the calculated structures. Final structure calculation was done with REDAC using 500 starting structures with randomized torsion angles. Within the first 100 conformers with lowest target function, no clear jump could be detected in the final target-function value. Because no different conformational subfamilies were present within the first 50 calculated conformers, the 25 conformers with lowest target function were arbitrarily selected for further restrained energy refinement. The N-terminal acetyl group was attached. Because the distance restraints to this group were not restraining (sequential type only), these were not included during the refinement process.

Structures were refined with a simulated annealing protocol in the AMBER force field (Weiner et al. 1984) as implemented in DISCOVER (version 2.98, Accelrys, Inc.). Distance and angle restraints were used (force constant: 32 kcal/mole.Å^2) as well as peptide-bond planarity restraints (100 kcal/mole.rad^2). Hydrogen-bond restraints were omitted. Prior to refinement, angles defined by multiple angle restraints in DYANA were converted to single-angle restraints. Chirality restraints were added (100 kcal/mole.rad^2). After initial rEM with 100 steps of steepest descents and 500 steps of conjugate gradients minimization, rMD was applied during 5 psec at 1000 K, followed by cooling to 300 K in steps of 100 K, with 1-psec simulation time at every temperature. At 300 K, an additional 5 psec of rMD was performed. Finally, a rEM was applied with 100 steps of steepest descents and 1000 steps of conjugate gradient, until the maximum gradient of the AMBER energy was smaller than 0.001 kcal/mole.Å^2. A Lennard-Jones potential was used throughout with a 100 Å cutoff. A distance-dependent dielectric constant ($\epsilon_0 = 4$) was used.

The refined structures were validated using the software packages PROCHECK-NMR, AQUA (Laskowski et al. 1996) and WhatIf (Vriend et al. 1990). Secondary structure classification was done by the method of Kabsch and Sander (1983) as implemented in PROCHECK-NMR. Calculated structures were displayed and analyzed using the molecular graphics programs InsightII, MOLMOL (Koradi et al. 1996), and PyMOL (http://www.pymol.org).

Data bank accession numbers

The coordinates of both refined ensembles have been deposited in the EBI Protein DataBase under accession ID code 1UNC and 1UND for HVcHP and HAcHP, respectively. Chemical shifts have been deposited in the BioMagRes Bank under accession codes 5964, 5965, and 5966 for HVcHP, HVcHP W64A, and HAcHP, respectively.

Acknowledgments

We thank C. Mihai and Prof. R. Willem from the high-resolution NMR center of the University of Brussels for fruitful discussions during the refinement process. We also thank D. Dewitte for technical assistance and S. Rossenu for performing initial cross-linking experiments. This work was supported by the Fund for Scientific Research-Flanders (F.W.O.) through a fellowship to W.V., a postdoctoral fellowship to M.V.T., NMR equipment grants (G.0036.00N, G.0365.03), and a research grant (G.0007.03) to C.A. Additional support came from the Concerted Research Actions of the Flemish Community by a GOA grant (12051401) to Joël Vandekerckhove (Department of Biochemistry, Faculty of Medicine) and C.A.

The publication costs of this article were defrayed in part by payment of page charges. This article must therefore be hereby marked "advertisement" in accordance with 18 USC section 1734 solely to indicate this fact.

References

Arpin, M., Pringault, E., Finidori, J., Garcia, A., Jeltsch, J.-M., Vandekerckhove, J., and Louvard, D. 1988. Sequence of human villin—a large duplicated domain homologous with other actin-severing proteins and a unique small carboxy-terminal domain related to villin specificity. *J. Cell. Biol.* **107:** 1759–1766.

Bazari, W.L., Matsudaira, P.T., Wallek, M., Smeal, T., and Jakes, R. 1988. Villin sequence and peptide map identify 6 homologous domains. *Proc. Natl. Acad. Sci.* **85:** 4986–4990.

Bretscher, A. and Weber, K. 1980. Villin is a major protein of the microvillus cytoskeleton which binds both G- and F-actin in a calcium-dependent manner. *Cell* **20:** 839–847.

Case, D.A. 1995. Calibration of ring-current effects in proteins and nucleic acids. *J. Biomol. NMR* **6:** 341–346.

Craig, S.W. and Powell, L.D. 1980. Regulation of actin polymerization by villin, a 95,000 Dalton cytoskeletal component of intestinal brush-borders. *Cell* **22:** 739–746.

Doering, D.S. and Matsudaira, P.T. 1996. Cysteine scanning mutagenesis at 40 of 76 positions in villin headpiece maps the F-actin binding site and structural features of the domain. *Biochemistry* **35:** 12677–12685.

Eberstadt, M., Gremmecker, G., Mierke, D., and Kessler, H. 1995. Scalar coupling-constants—their analysis and their application for the elucidation of structures. *Angew. Chem. Int. Ed. Engl.* **34:** 1671–1695.

Friederich, E., Vancompernolle, K., Huet, C., Goethals, M., Finidori, J., Vandekerckhove, J., and Louvard, D. 1992. An actin-binding site containing a conserved motif of charged amino acid residues is essential for the morphogenic effect of villin. *Cell* **70:** 81–92.

Glenney Jr., J.R., and Weber, K. 1981. Calcium control of microfilaments—uncoupling the F-actin severing and F-actin bundling activity of villin by limited proteolysis in vitro. *Proc. Natl. Acad. Sci.* **78:** 2810–2814.

Glenney Jr., J.R., Kaulfus, P., and Weber, K. 1981. F-actin assembly modulated by villin—Ca^{2+} dependent nucleation and capping of the barbed end. *Cell* **24:** 471–480.

Griesinger, C., Sørensen, O., and Ernst, R. 1985. Two-dimensional correlation of connected NMR transitions. *J. Am. Chem. Soc.* **110:** 7870–7872.

Griesinger, C., Otting, G., Wüthrich, K., and Ernst, R.R. 1988. Clean TOCSY for ^{1}H spin system identification in macromolecules. *J. Am. Chem. Soc.* **110:** 7870–7872.

Güntert, P., Mumenthaler, C., and Wüthrich, K. 1997. Torsion angle dynamics for NMR structure calculation with the new program DYANA. *J. Mol. Biol.* **273:** 283–298.

Kabsch, W. and Sander, C. 1983. Dictionary of protein secondary structure–pattern recognition of hydrogen bonded and geometrical features. *Biopolymers* **A47:** 392–400.

Kessler, H. and Oschkinat, H. 1985. Simplification of spectra for the determination of coupling-constants from homonuclear correlated 2D NMR spectra. *Angew. Chem. Int. Ed. Engl.* **24:** 690–692.

Kim, Y. and Prestegard, J.H. 1989. Measurement of vicinal couplings from cross peaks in COSY spectra. *J. Magn. Reson.* **84:** 9–13.

Kjær, M., Andersen, K.V., and Poulsen, F.M. 1994. Automated and semiautomated analysis of homo- and heteronuclear multidimensional nuclear magnetic resonance spectra of proteins: The program PRONTO. *Methods Enzymol.* **239:** 288–308.

Koradi, R., Billeter, M., and Wüthrich, K. 1996. MOLMOL: A program for display and analysis of macromolecular structures. *J. Mol. Graph.* **14:** 51–55.

Kumar, A., Wagner, G., Ernst, R.R., and Wüthrich, K. 1980. Studies of J-connectivities and ^{1}H-^{1}H Overhauser effects in H_2O solutions of biological macromolecules by two-dimensional NMR experiments. *Biochem. Biophys. Res. Comm.* **96:** 1156–1163.

Laskowski, R.A., Rullmann, J.A.C., MacArthur, M.W., Kaptein, R., and Thornton, J. 1996. AQUA and PROCHECK-NMR: Programs for checking the quality of protein structures solved by NMR. *J. Biomol. NMR* **8:** 477–486.

Marion, D. and Wüthrich, K. 1983. Application of phase-sensitive two-dimensional correlated spectroscopy (COSY) for measurements of ^{1}H-^{1}H spin coupling constants in proteins. *Biochem. Biophys. Res. Comm.* **113:** 967–974.

Marion, D., Ikura, M., and Bax, A. 1989. Improved solvent suppression in one-dimensional and two-dimensional NMR-spectra by convolution of time-domain data. *J. Magn. Res.* **84:** 425–430.

Marion, D., Ikura, M., Tschudin, R., and Bax, A. 1991. Rapid recording of 2D-NMR spectra without phase cycling—application to the study of hydrogen exchange in proteins. *J. Magn. Reson.* **85:** 393–399.

Markley, J.L., Bax, A., Arata, Y., Hilbers, C.W., Kaptein, R., Sykes, B.D., Wright, P.E., and Wüthrich, K. 1998. Recommendations for the presentation of NMR structures of proteins and nucleic acids. *Pure Appl. Chem.* **70:** 117–142.

McKnight, C.J., Doering, D.S., Matsudaira, P.T., and Kim, P.S. 1996. A thermostable 35-residue subdomain within villin headpiece. *J. Mol. Biol.* **260:** 126–134.

McKnight, C.J., Matsudaira, P.T., and Kim, P.S. 1997. NMR structure of the 35-residue villin headpiece subdomain. *Nat. Struct. Biol.* **4:** 180–184.

Mooseker, M.S., Graves, T.A., Wharton, K.A., Falco, N., and Howe, C.L. 1980. Regulation of microvillus structure—calcium-dependent solation and cross-linking of actin filaments in the microvilli of intestinal epithelial cells. *J. Cell. Biol.* **87:** 809–822.

Nagayama, K. and Wüthrich, K. 1981. Structural interpretation of vicinal proton-proton coupling-constants $^{3}J_{H\alpha H\beta}$ in the basic pancreatic trypsin-inhibitor measured by two-dimensional J-resolved NMR spectroscopy. *Eur. J. Biochem.* **115:** 653–657.

Neuhaus, D., Wagner, G., Vašák, M., Kagi, J.H.R., and Wüthrich, K. 1985. Systematic application of high-resolution, phase sensitive two-dimensional ^{1}H NMR techniques for the identification of the amino-acid-proton spin systems in proteins–rabbit methallothionein-2. *Eur. J. Biochem.* **151:** 257–273.

Osapay, K. and Case, D.A. 1991. A new analysis of proton chemical-shifts in proteins. *J. Am. Chem. Soc.* **113:** 9436–9444.

Piotto, M., Saudek, V., and Sklenar, V. 1992. Gradient-tailored excitation for single-quantum NMR spectroscopy of aqueous solutions. *J. Biomol. NMR* **2:** 661–665.

Rance, M., Bodenhausen, G., Wagner, G., Ernst, R.R., and Wüthrich, K. 1984. Improved spectral resolution in COSY ^{1}H NMR spectra of proteins via double quantum filtering *Biochem. Biophys. Res. Comm.* **117:** 479–785.

Ravenall, S.J., Gavazzi, I., Wood, J.N., and Akopian, A.N. 2002. A peripheral nervous system actin-binding protein regulates neurite outgrowth. *Eur. J. Neurosci.* **15:** 281–290.

Roof, D.J., Hayes, A., Adamian, M., Chishti, A., and Li, T. 1997. Molecular characterization of abLIM, a novel actin-binding and double zinc finger protein. *J. Cell. Biol.* **138:** 575–588.

Rossenu, S., Leyman, S., Dewitte, D., Peelaers, D., Jonckheere, V., Van Troys, M., Vandekerckhove, J., and Ampe, C. 2003. A phage display based method for determination of relative affinities of mutants; application to the actin binding motifs in thymosin β4 and villin headpiece. *J. Biol. Chem.* **278:** 16642–16650.

Shimizu, A., Ikeguchi, M., and Sugai, S. 1994. Appropriateness of DSS and TSP as internal references for ^{1}H NMR studies of molten globule proteins in aqueous media. *J. Biomol. NMR* **4:** 859–862.

Spudich, J.A. and Watt, S. 1971. The regulation of rabbit skeletal muscle contraction. I. Biochemical studies of the interaction of the tropomyosin-troponin complex with actin and with the proteolytic fragments of myosin. *J. Biol. Chem.* **246:** 4866–4871.

Vancompernolle, K., Goethals, M., Huet, C., Louvard, D., and Vandekerckhove, J. 1992. G- to F-actin modulation by a single amino acid substitution in the actin binding site of actobindin & thymosin β4. *EMBO J.* **11:** 4739–4746.

Van Troys, M., Dewitte, D., Goethals, M., Carlier, M.F., Vandekerckhove, J., and Ampe, C. 1996. The actin binding site of thymosin β4 mapped by mutational analysis. *EMBO J.* **15:** 201–210.

Vardar, D., Buckley, D.A., Frank, B.S., and McKnight, C.J. 1999. NMR structure of an F-actin-binding "headpiece" motif from villin. *J. Mol. Biol.* **294:** 1299–1310.

Vardar, D., Chishti, A.H., Frank, B.S., Luna, E.J., Noegel, A.A., Oh, S.W., Schleicher, M., and McKnight, C.J. 2002. Villin-type headpiece domains show a wide range of F-actin-binding affinities. *Cell Motil. Cytoskel.* **52:** 9–21.

Vriend, G. 1990. What If–a molecular modelling and drug design program. *J. Mol. Graph.* **8:** 52–56.

Weiner, S.J., Kollman, P.A., Case, D.A., Singh, C., Ghio, C., Alagona, G., Profeta, S., and Weiner, P. 1984. A new force field for molecular mechanical simulation of nucleic acids and proteins. *J. Am. Chem. Soc.* **106:** 765–784.

Widmer, H., Billeter, M., and Wüthrich, K. 1989. Three-dimensional structure of the neurotoxin ATX Ia from *Anemonia sulcata* in aqueous solution determined by nuclear magnetic resonance spectroscopy. *Proteins* **6:** 357–371.

Wilmot, C.M. and Thornton, J.M. 1990. β-Sheets and their distortions—a proposed new nomenclature. *Protein Eng.* **3:** 479–493.

Wishart, D.S. and Nip, A.M. 1998. Protein chemical shift analysis: A practical guide. *Biochem. Cell. Biol.* **76:** 153–163.

Wishart, D.S., Sykes, B.D., and Richards, F.M. 1992. The chemical shift index—a fast and simple method for the assignment of protein secondary structure through NMR spectroscopy. *Biochemistry* **31:** 1647–1651.

Wishart, D.S., Bigam, C.G., Yao, J., Abildgaard, F., Dyson, H.J., Oldfield, E., Markley, J.L., and Sykes, B.D. 1995. ^{1}H, ^{13}C and ^{15}N chemical shift referencing in biomolecular NMR. *J. Biomol. NMR* **6:** 135–140.

Wüthrich, K. 1986. *NMR of proteins and nucleic acids.* Wiley-Interscience, New York.

Wüthrich, K., Billeter, M., and Braun, W. 1983. Pseudo-structures for the 20 common amino-acids for use in studies of protein conformations by measurements of intramolecular proton proton distance constraints with nuclear magnetic resonance. *J. Mol. Biol.* **169:** 949–961.

Zhai, L., Zhao, P., Panebra, A., Guerrerio, A.L., and Khurana, S. 2001. Tyrosine phosphorylation of villin regulates the organisation of the actin cytoskeleton. *J. Biol. Chem.* **276:** 36163–36167.